Landes Bioscience www.landesbioscience.com

Supplemental Material to:

Vangelis Kondylis, Hezder E. van Nispen tot Pannerden, Suzanne van Dijk, Toine ten Broeke, Richard Wubbolts, Willie J. Geerts, Cor Seinen, Tuna Mutis and Harry F.G. Heijnen

Endosome-mediated autophagy: An unconventional MIIC-driven autophagic pathway operational in dendritic cells

Autophagy 2013; 9(6)
http://dx.doi.org/10.4161/auto.24111

www.landesbioscience.com/journals/autophagy/article/24111

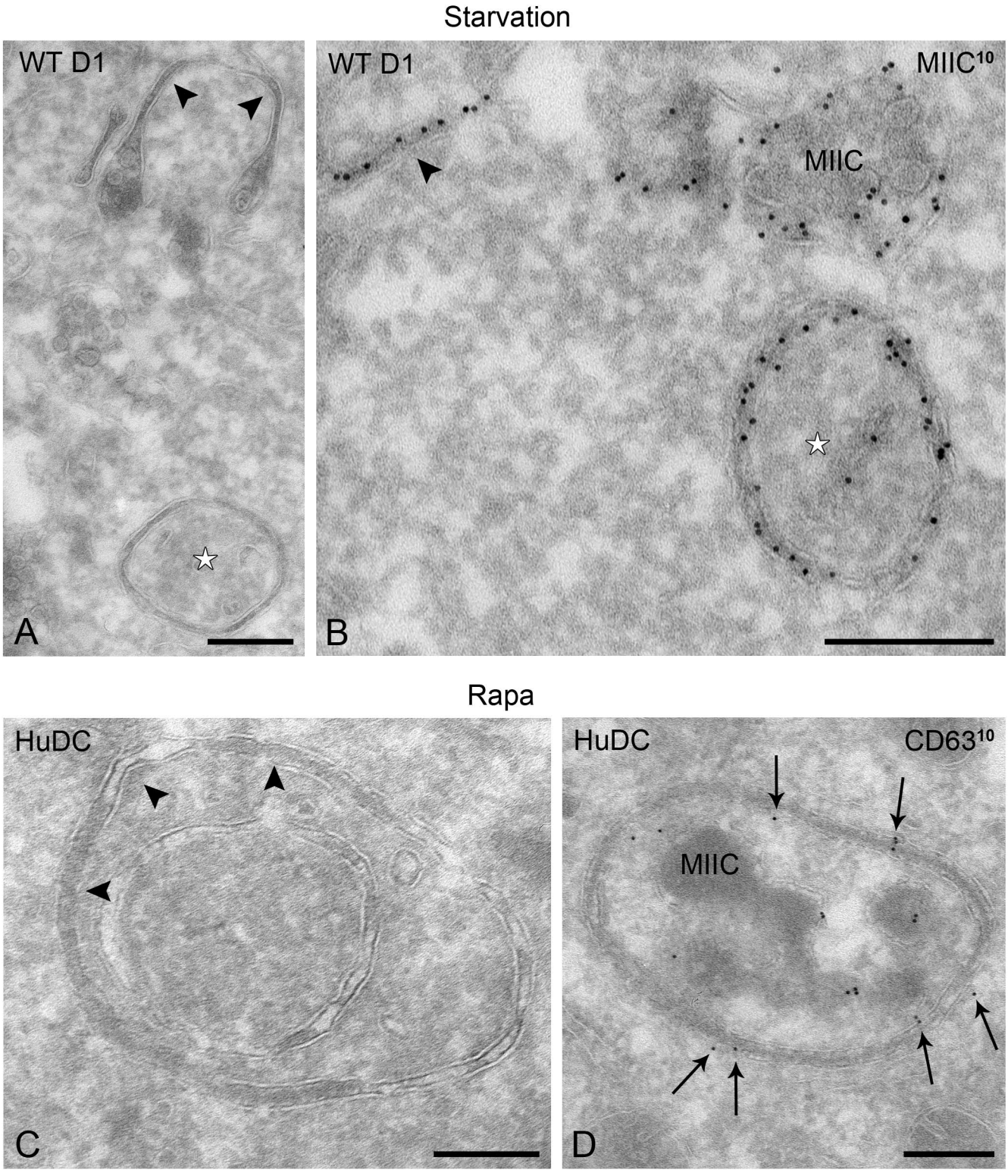
Starvation
WT D1
WT D1
MIIC10
MIIC
A
B
Rapa
HuDC
HuDC
CD6310
MIIC
C
D

Figure S1

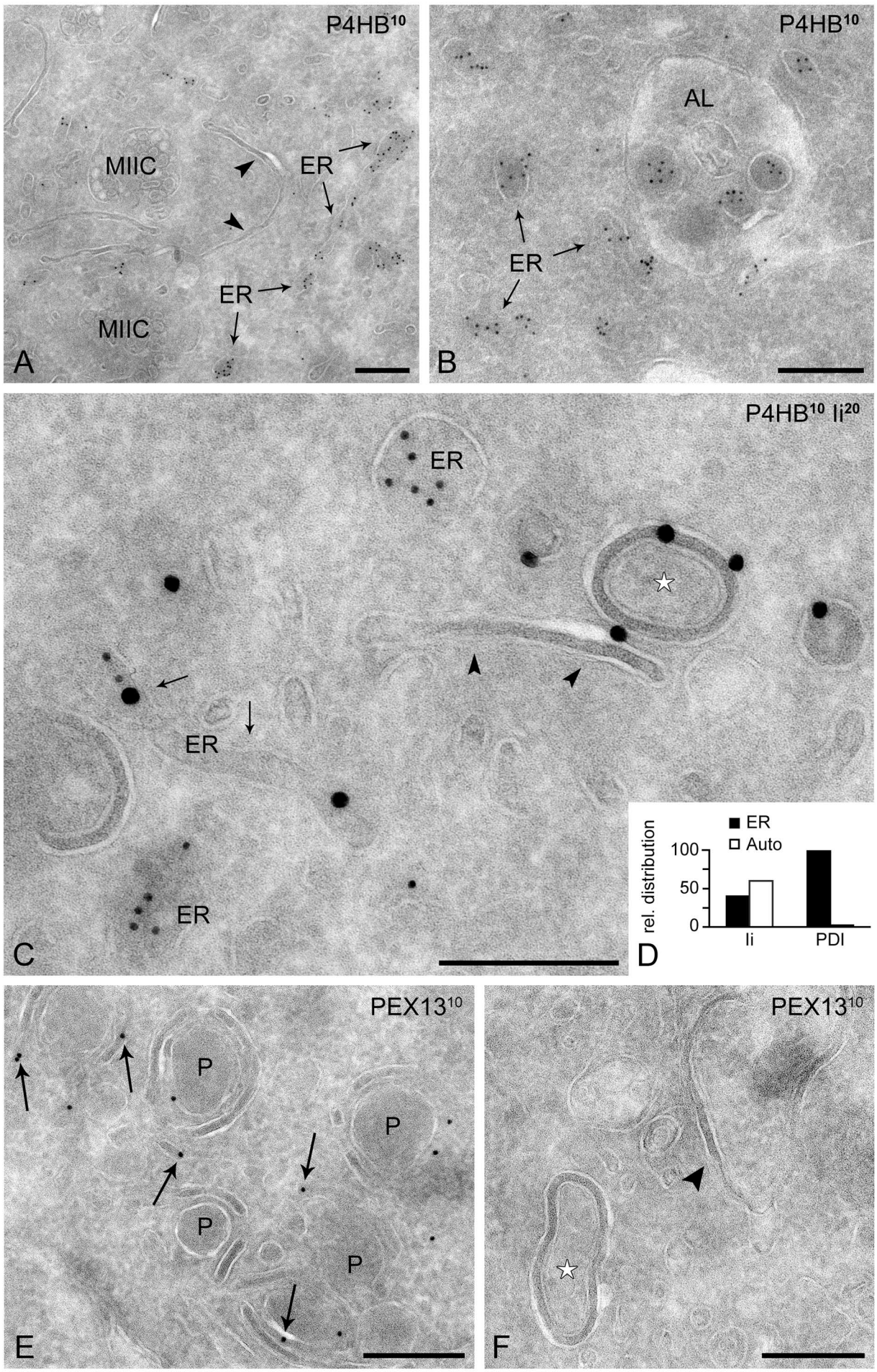
6h LPS/BAFA1
P4HB10
MIIC
ER
ER
MIIC
A
P4HB10
AL
ER
B
P4HB10 Ii20
ER
ER
ER
C
rel. distribution
ER
Auto
100
50
0
Ii
PDI
D
PEX1310
P
P
P
P
E
PEX1310
F

Figure S2

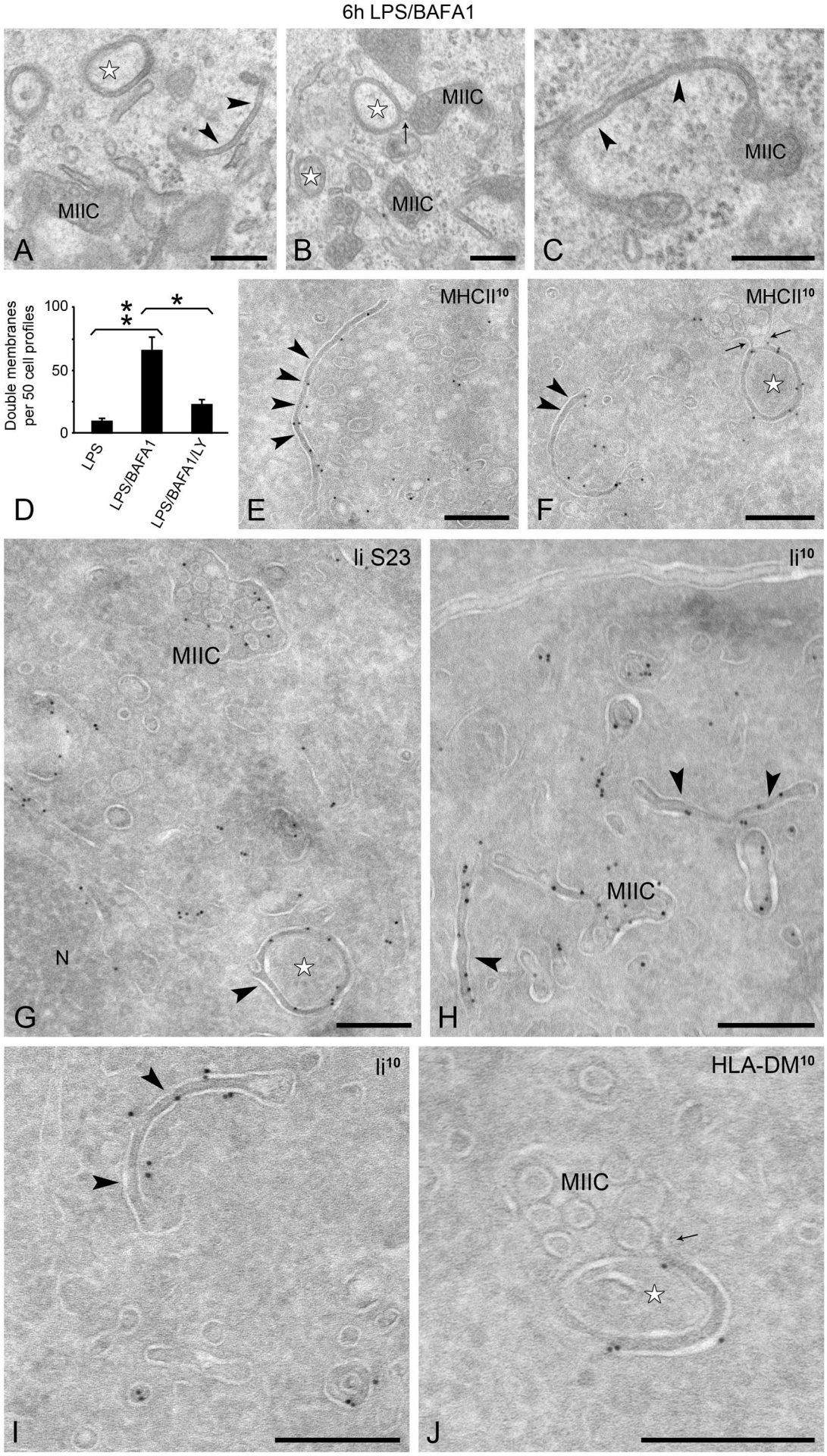
6h LPS/BAFA1
MIIC
A
MIIC
MIIC
B
MIIC
C
Double membranes per 50 cell profiles
100
50
0
**
*
LPS
LPS/BAFA1
LPS/BAFA1/LY
D
MHCII10
E
MHCII10
F
li S23
MIIC
N
G
li10
MIIC
H
li10
I
HLA-DM10
MIIC
J

Figure S3

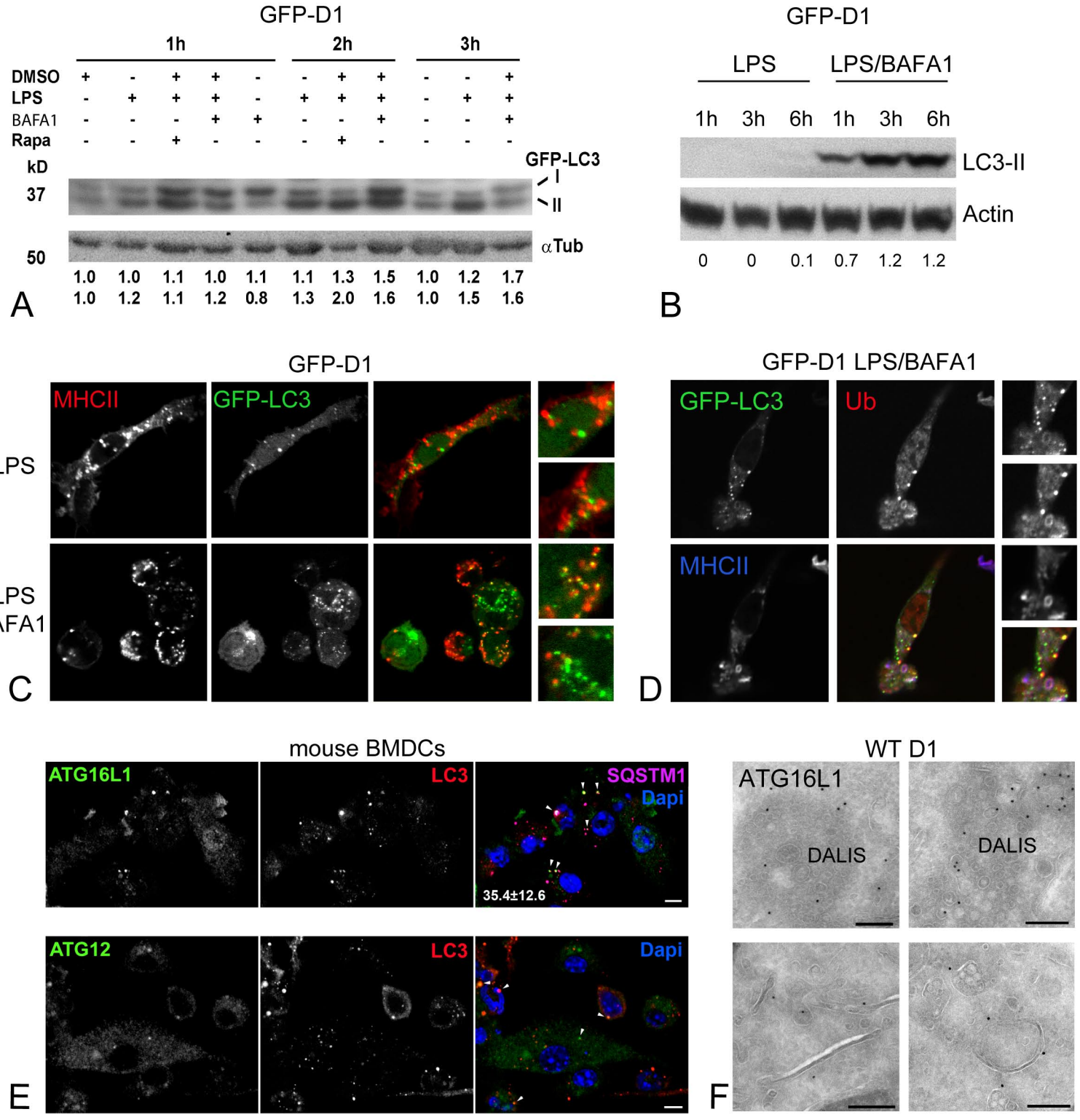
GFP-D1
1h
2h
3h
DMSO
LPS
BAFA1
Rapa
kD
37
50
GFP-LC3
I
II
αTub
1.0 1.0 1.1 1.0 1.1 1.1 1.3 1.5 1.0 1.2 1.7
1.0 1.2 1.1 1.2 0.8 1.3 2.0 1.6 1.0 1.5 1.6
A
GFP-D1
LPS
LPS/BAFA1
1h 3h 6h 1h 3h 6h
LC3-II
Actin
0 0 0.1 0.7 1.2 1.2
B
GFP-D1
MHCII
GFP-LC3
LPS
LPS
BAFA1
C
GFP-D1 LPS/BAFA1
GFP-LC3
Ub
MHCII
D
mouse BMDCs
ATG16L1
LC3
SQSTM1
Dapi
35.4±12.6
ATG12
LC3
Dapi
E
WT D1
ATG16L1
DALIS
DALIS
F

Figure S4

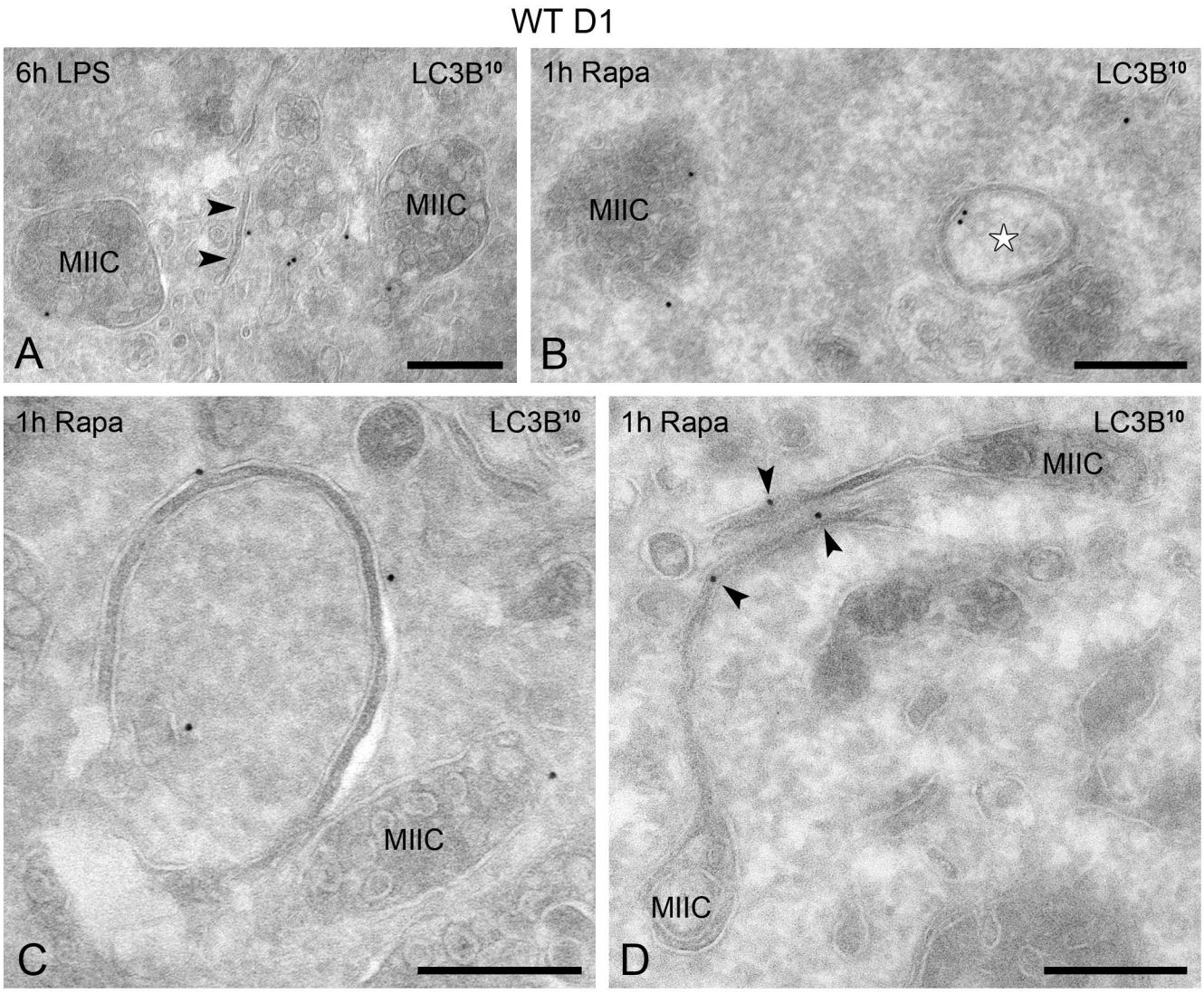
WT D1
6h LPS
LC3B10
MIIC
MIIC
A
1h Rapa
LC3B10
MIIC
B
1h Rapa
LC3B10
MIIC
C
1h Rapa
LC3B10
MIIC
MIIC
D

Figure S5

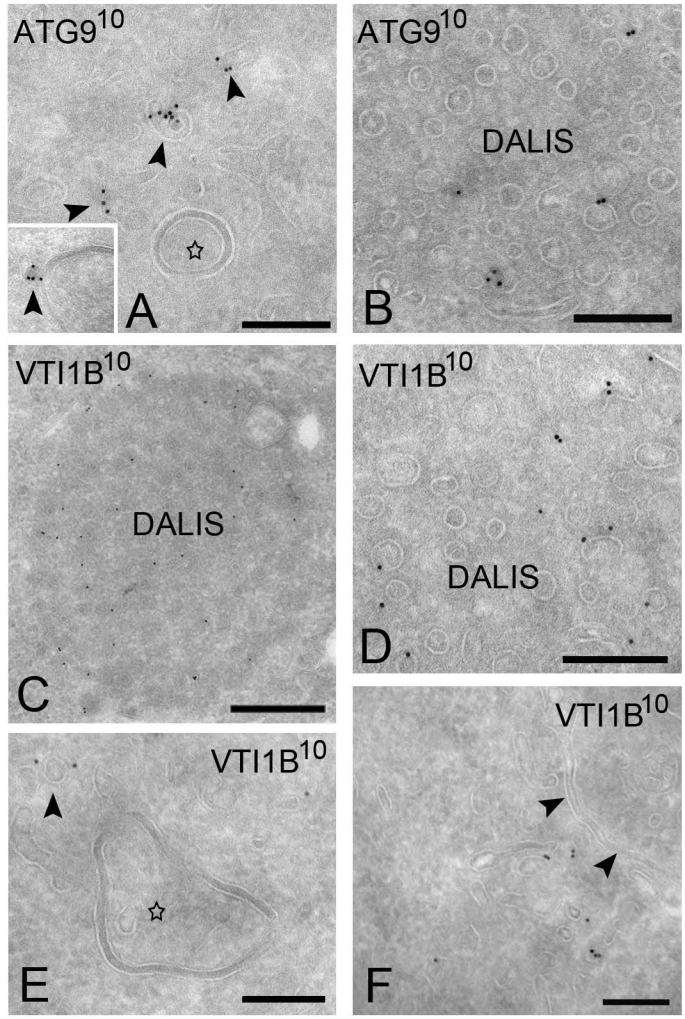
ATG9^{10}
A
ATG9^{10}
DALIS
B
VTI1B^{10}
DALIS
C
VTI1B^{10}
DALIS
D
VTI1B^{10}
E
VTI1B^{10}
F

Figure S6

Figure S1. Autophagosomes induced by nutrient starvation or rapamycin in DCs contain late endosomal markers. (**A and B**) WT D1 cells were starved for 30 min in D-PBS. Classical autophagosome profiles (stars) and highly curved phagophores (arrowheads) containing high amounts of MHC class II were frequently observed. Note in B the close association of the autophagosome to an MIIC. (**C and D**) Monocyte-derived human DCs were treated for 60 min with rapamycin. The arrowheads indicate typical double-membrane autophagosomal structures that are positive for the late-endosomal marker CD63 (arrows). Bars, 200 nm.

Figure S2. General ER or specialized ER subdomains that give rise to peroxisomes, do not supply the autophagosome membrane. Immuno-localization of P4HB (protein disulfide isomerase) (**A–D**) and PEX13 (**E and F**) in D1 cells incubated with LPS in the presence of BAFA1. (**A**) P4HB is in distinct RER cisternae (arrows) and not associated with autophagic structures (arrowheads). (**B**) P4HB-positive membranes are recovered in autolysosmes (AL), suggestive of ER turnover by autophagy. (**C**) Double labeling for P4HB (10nm gold) and Invariant chain (Ii, 20 nm gold) shows partial colocalization in certain ER cisternae (arrows), but also segregation in other ER subdomains (ER) and double membrane structures (arrowheads and star). Note the close association of ER cisternae with the double-membrane structure. (**D**) Quantification of PDI and Ii relative distribution on ER and autophagic membranes. (**E and F**) The peroxisomal marker PEX13 is exclusively associated with the peroxisome-connected lamellae (arrows) that emerge from the ER (**E**), but not with autophagosomes (star and arrowhead in **F**). As previously shown (ref 31), the electron-dense lamellar ER subdomains are always associated with peroxisomes (P) and rarely with MIICs. Bars, 200 nm.

Figure S3. LPS-stimulated GFP-LC3 D1 cells exhibit double-membrane structures containing MIIC-specific molecular markers. GFP-LC3 expressing D1 cells were incubated for 6 h with LPS in the presence of BAFA1. (**A–C**) Representative electron micrographs of autophagosomes (stars) and phagophores (arrowheads). (**D**) Quantitation of double-membrane structures in GFP-LC3 D1 cells under various experimental conditions. Data represent the mean of 3 independent experiments ±SD (*$p < 0.04$; **$p < 0.01$). (**E–J**) Double-membrane profiles labeled for MHC class II (arrowheads in **E and F**), Ii (**G–I**), and HLA-DM (**J**). Note the continuity between the double-membrane structures and MIIC profiles (arrows in **B, F and J**). Ii, Invariant chain, lumenal domain; Ii S23, Invariant chain, cytosolic domain; MIIC, MHC class II compartment. Bars, 200 nm.

Figure S4. Behavior of autophagosomal markers upon LPS and LPS/BAFA1 stimulation. (**A**) Immunoblot of whole-cell lysates from GFP-LC3 D1 cells treated as indicated. GFP-LC3-I and GFP-LC3-II were detected with an anti-GFP antibody. α-Tubulin/TUBA was used as loading control. Quantification of LC3-I/α-Tubulin and LC3-II/α-Tubulin ratio was performed using ImageJ. The numbers represent fold increase compared to the ratio of the control samples for each time point, which were set at 1. The image is representative from 3 independent experiments. Note that LC3-II/α-Tubulin ratio increases mildly upon LPS stimulation but not as strongly as for LPS/BAFA1 or LPS/rapamycin. Note that BAFA1 treatment seems to increase also LC3-I (lane 5). (**B**) Immunoblot in GFP-LC3 D1 cells treated as indicated. Endogenous LC3 was detected with an anti-LC3 antibody. Quantification of LC3-II/actin was performed as in A. **(C)** Localization of GFP-LC3 in relation to MHC class II upon LPS-stimulation for 6 h in the absence or presence of BAFA1. Note that BAFA1 resulted in increased but not complete overlap of LC3 puncta with MHC class II. **(D)** Localization of GFP-LC3 compared to ubiquitinated structures/proteins and MHC class II upon stimulation with LPS/BAFA1 for 6 h. Note that GFP-LC3 colocalizes significantly with ubiquitin-positive puncta, but much less with MHC class II compartments. (**E**) BMDCs stimulated with LPS/BAFA1 for 8 h showing partial colocalization of LC3 with ATG16L1 and ATG12. The percentage of ATG16L1 puncta that colocalize with LC3 is mentioned. (**F**) IEM localization of ATG16L1 in small vesicular assemblies representing DALIS and early autophagic structures. Bars, 200 nm.

Figure S5. Immuno-EM localization of endogenous LC3. Representative electron micrographs showing low but specific immunogold localization of LC3B on phagophores (arrowheads in **A and D**), autophagosomes (**B and C**), and MIICs (**A–C**) in WT D1 cells. (**A**) 6 h LPS, (**B–D**) 1 h rapamycin. Bars, 200 nm.

Figure S6. Immuno-EM localization of ATG9 and VTI1B. (**A and B**) Electron micrographs showing ATG9 localization on vesicular membranes (arrowheads) in close proximity to an autophagosome (star in **A**), and to a lesser extent in DALIS (**B**). Inset in (**A**) shows an ATG9-positive vesicle in continuity with the double-membrane structure. (**C and D**) Immunogold localization of VTI1B on vesicles located in DALIS. (**E and F**) Immunogold localization of VTI1B on small vesicular membranes in close proximity to the double-membrane structures (star in **E**) and MIIC-connected phagophores (arrowheads in **F**). Bars, 200 nm.

Movie S1

WT D1 upon 6 h stimulation with LPS. Tomographic representation and 3D reconstruction of a putative phagophore, connected to a multivesicular MIIC-like structure. Note that this compartment contains internal vesicular and sheet-like membranes.

Movie S2

WT D1 upon 6 h stimulation with LPS. Tomographic reconstruction and 3D model of a cup-shaped double-membrane structure. Note the very regular shape of the double membranes and the vesicles contained within the two round membranes. The concave membranes engulf cytoplasmic material and isolated membrane vesicles.

Movie S3

WT D1 upon 6 h stimulation with LPS. Characteristic double-membrane structure reminiscent of an autophagosome. Note the small connection between the multilaminar and reticular MIIC in the right upper corner. The double membranes have sequestered cytoplasmic material, including small organelles and ribosomes. A ~20-nm gap in the double-membrane structure still retains connection with the cytosol. From the double membrane a tubular extension stretches into the cytoplasm.

Movie S4

WT D1 after 6 h stimulation with LPS in the presence of BAFA1. Tomographic representation and 3D reconstructed model of autophagosome connected to multivesicular MIIC.

Movie S5

WT D1 after 6 h stimulation with LPS in the presence of BAFA1. Tomographic representation and 3D reconstructed model of autophagosome connected to multivesicular MIIC.

Movie S6

WT D1 after 6 h stimulation with LPS in the presence of BAFA1. Immunogold labeling using anti-SQSTM1 antibody and 10-nm protein-A gold. Tomographic representation and 3D reconstruction of SQSTM1-DALIS engulfment by MIIC-driven double-membrane structure.

Movie S7

mStrawberry-ATG4B^{C74A} D1 after 6 h stimulation with LPS in the presence of BAFA1. Tomographic representation and 3D reconstructed model of phagophores and autophagosomes connected to multivesicular MIICs.

Movie S8

mStrawberry-ATG4B^{C74A} D1 after 6 h stimulation with LPS in the presence of BAFA1. Tomographic representation and 3D reconstructed model of characteristic MIIC (yellow) and almost closed autophagosome (blue).